ELSEVIER

Original article

3D-QSAR studies of indole derivatives as phosphodiesterase IV inhibitors

Asit K. Chakraborti *, B. Gopalakrishnan, M. Elizabeth Sobhia, Alpeshkumar Malde

*Department of Medicinal Chemistry, National Institute of Pharmaceutical Education and Research (NIPER),
Sector-67, S.A.S. Nagar 160 062, Punjab, India*

Abstract

The 3D-QSAR studies of some indole derivatives as phosphodiesterase (PDE) type IV inhibitors was performed by Comparative Molecular Field Analysis (CoMFA) and Comparative Molecular Similarity Indices Analysis (CoMSIA) methods to determine the factors required for the activity of these compounds. The global minimum energy conformer of the template molecule, **3** the most active molecule of the series, was obtained by simulated annealing method and used to build the structures of the molecules in the dataset. The CoMFA model produced statistically significant results with cross-validated and conventional correlation coefficients of 0.494 and 0.986 respectively. The combination of steric, electrostatic and hydrophobic fields in CoMSIA gave the best results with cross-validated and conventional correlation coefficients of 0.541 and 0.967 respectively. The predictive ability of CoMFA and CoMSIA were determined using a test set of seven indole derivatives giving predictive correlation coefficients of 0.56 and 0.59 respectively indicating good predictive power. Further, the robustness of the models was verified by bootstrapping analysis. Based upon the information derived from CoMFA and CoMSIA, we have identified some key features that may be used to design new indole derivatives and predict their PDE IV affinities prior to synthesis.

1. Introduction

Interest in the potential utility of isoenzyme selective phosphodiesterase (PDE) inhibitors has increased in recent years [1]. At least 11 families of PDE based upon a variety of criteria including substrate specificity, inhibition potency, enzyme kinetics, amino acid sequence, cellular and tissue distribution are known to exist [2]. Many pharmaceutical companies are attempting to discover the magic bullet for diseases like asthma and chronic obstructive pulmonary disease (COPD) [3]. In this context, PDE type IV has been selectively targeted using chemical inhibitors on the basis of the clinical efficacy of the archetypal non-selective PDE inhibitor, theophylline, which has been used in the treatment of asthma and COPD [4]. PDE IV is a cyclic adenosine mono-phosphate (c-AMP) specific enzyme

showing very low affinity for cGMP [5]. The inhibition of PDE IV activity increases the cellular level of cyclic adenosine 5′-monophosphate (c-AMP), thereby activating specific protein phosphorylation cascades that elicit variety of functional responses in the inflammatory cells and bronchial smooth muscles [6]. The archetypal inhibitor rolipram [7] (Scheme 1) has been the starting point for the majority of the medicinal chemistry efforts. The research in this area dealing with the replacement of pyrrolidinone of rolipram with other functionalities led to discovery of piclamilast (RP-73401) [8]. However, piclamilast was discontinued at phase two clinical trials due to undesirable side effects and poor pharmacokinetics [9]. The design of rigid analogs of piclamilast led to a series of indole class of PDE IV inhibitors. The replacement of catechol like rolipram motif of piclamilast with indole nucleus represents one of the first conformationally constrained analogues. Indole nucleus was found to be an effective isostere for catechol of

---

* Correspondence author.
E-mail address: akchakraborti@niper.ac.in (A.K. Chakraborti).

Rolipram

Piclamilast
(RP 73401)
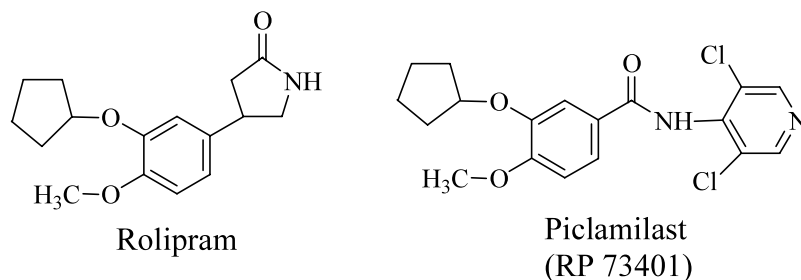
Scheme 1.

piclamilast. Indole derivatives also showed improved pharmacokinetics [10,11].

Although the three-dimensional structure of the native PDE IV enzyme in the solid state has been recently reported [12], the experimental data on the PDE IV-inhibitor complex is not available. In such circumstances, the indirect approach i.e. ligand based approaches like 3D-QSAR studies are quite useful for lead optimization and drug design. Recently, we have reported the 3D-QSAR study of PDE IV inhibitors belonging to thieno[3,2-d]pyrimidines [13]. We report herein the results of comparative molecular field analysis (CoMFA) and comparative molecular similarity indices analysis (CoMSIA) performed on a series of indole as PDE IV inhibitors (Table 1). The 3D-QSAR analyses can provide more insight into the optimization of this series of PDE IV inhibitors. Since its introduction in 1988, CoMFA [14] has rapidly become one of the most powerful tools for 3D-QSAR studies [15,16]. CoMFA methodology is based on the assumption that the changes in the biological activity correlate with the changes in the steric and electrostatic fields of the molecules. The CoMSIA [17] method differs by the way the molecular fields are calculated and by including additional molecular fields, such as lipophilic and hydrogen bond potential. The additional fields in CoMSIA provide better visualization and interpretation of the obtained correlation in terms of field contribution to the activity of the compound. On the basis of CoMFA and CoMSIA models for indole derivatives, we attempted to elucidate a structure–activity relationship to provide useful information for the design and synthesis of more potent indoles and related derivatives with predetermined affinities.
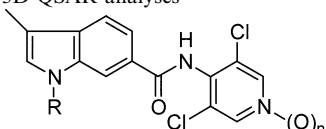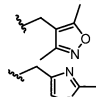
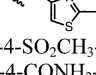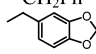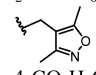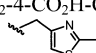## 2. Results and discussion

The CoMFA model obtained with 28 indole derivatives in training set resulted in a six-component model with cross-validated correlation coefficient of 0.494 and minimum standard error. This analysis was used for final non-cross validated run, giving a correlation coefficient of 0.986 giving a good linear correlation

between the observed and predicted activities of the molecules in the training set. To test the predictive ability of the resulting model, a test set of seven molecules excluded from the model creation work was used. The predictive correlation coefficient of 0.56 was obtained for CoMFA model. A high r^2 value of 0.992 during 100 runs of bootstrapped [18,19] analysis further supports the statistical validity of the model. The results of PLS analysis for CoMFA and CoMSIA are shown in Table 2. The alignment of the training set molecules is shown in Fig. 1. The relative contributions of steric and electrostatic fields for CoMFA are in the ratio 6:4. Steric interactions of molecule with active site of the enzyme could be an important factor for PDE IV inhibitory activity. A plot of predicted (CoMFA) versus actual activity for training set molecules is shown in Fig. 2. The test set residuals of CoMFA and CoMSIA analyses are shown in Fig. 3, while Fig. 4 represents the plot of predicted (CoMSIA) versus actual activity values. The actual, predicted and residual values of training and test set for CoMFA and CoMSIA are given in Tables 3 and 4 respectively. Contour maps were generated as scalar product of coefficients and standard deviation associated with each CoMFA column. The 3D-QSAR contour maps revealing the contribution of CoMFA and CoMSIA fields are shown in Figs. 5 and 6 respectively. The CoMFA steric interactions are represented by green (G) and yellow (Y) coloured contours while electrostatic interactions are represented by red (R) and blue (B) coloured contours. The bulky substituents are favoured in green regions and disfavoured in yellow (Y) regions. The increase in positive charge is favoured in blue (B) regions while the increase in negative charge is favoured in red (R) regions. The most active molecule **3** (template, IC$_{50}$ 3.2 nM) is displayed in the background of contours.

The electrostatic contours of CoMFA (Fig. 5) shows a red (R) contour enclosing the cyclohexyl ring of the template molecule, a red (R) contour away from the indole nucleus and two red (R) contours near dichloropyridine ring where high electron density is expected to increase the activity. The compound **12** (IC$_{50}$ 12 nM) with a 4-methoxybenzyl substituent exhibits good activity where the electronegative oxygen is buried in red (R)

Table 1
Dataset used for 3D-QSAR analyses

Molecule	R	n	IC$_{50}$(nM)
1	cC$_5$H$_9$	0	15
2	CH$_2$-c-C$_6$H$_{11}$	0	100
3	CH$_2$CH$_2$-c-C$_6$H$_{11}$	0	3.2
4	(CH$_2$)$_6$CH$_3$	0	25
5	CH$_2$Ph	0	18
6	CH$_2$-2-C$_{10}$H$_7$	0	5.2
7	CH$_2$CH$_2$Ph	0	70
8	CH$_2$CH$_2$CH$_2$Ph	0	25
9	CH$_2$-1-C$_{10}$H$_7$	0	46
10	CH$_2$-2-OCH$_3$-C$_6$H$_4$	0	80
11	CH$_2$-3-OCH$_3$-C$_6$H$_4$	0	60
12	CH$_2$-4-OCH$_3$-C$_6$H$_4$	0	12
13	(structure)	0	187
14	(structure)	0	42
15	CH$_2$-4-SO$_2$CH$_3$-C$_6$H$_4$	0	200
16	CH$_2$-4-CONH$_2$-C$_6$H$_4$	0	300
17	CH$_2$-3-NO$_2$-C$_6$H$_4$	0	52
18	SO$_2$(4-CH$_3$-C$_6$H$_4$)	0	45
19	cC$_6$H$_{11}$	1	19
20	CH$_2$-c-C$_6$H$_{11}$	1	30
21	CH$_2$CH$_2$-c-C$_6$H$_{11}$	1	4.1
22	CH$_2$CH$_2$CH$_2$-c-C$_6$H$_{11}$	1	16
23	CH$_2$-c-C$_7$H$_{13}$	1	20
24	CH$_2$Ph	1	8
25	(structure)	1	24
26	CH$_2$-4-CF$_3$-C$_6$H$_4$	1	14
27	CH$_2$CH$_2$CH$_2$Ph	1	7
28	CH$_2$CH$_2$CH$_2$CH$_2$Ph	1	46
29	CH$_2$-2-C$_{10}$H$_7$	1	22
30	CH(CH$_3$)$_2$	1	38
31	CH$_2$-4-SO$_2$CH$_3$-C$_6$H$_4$	1	260
32	CH$_2$-4-Cl-C$_6$H$_4$	1	12
33	(structure)	1	500
34	CH$_2$-4-CO$_2$H-C$_6$H$_4$	1	1400
35	(structure)	1	80

contour. The compounds **10** (IC$_{50}$ 80 nM) and **11** (IC$_{50}$ 60 nM), where the methoxy group is present at 2- and 3-position, on the benzyl group at N of indole, respectively exhibit relatively low activity as electronegative oxygen is oriented in less favoured position, away from red contours. The CF$_3$ substituent at 4-position of benzyl group in **26** (IC$_{50}$ 14 nM) is buried in red (R) contour, and hence it exhibits good activity. The introduction of N-oxide on the dichloropyridine ring increases the activity as revealed by activities of **20** (IC$_{50}$ 30 nM), **24** (IC$_{50}$ 8 nM) and **27** (IC$_{50}$ 7 nM), which are N-oxides of **2** (IC$_{50}$ 100 nM), **5** (IC$_{50}$ 18 nM) and **8** (IC$_{50}$ 25 nM) respectively. The N-oxide increases the electron density in the region of red (R) contours near dichloropyridine

ring. The electrostatic contours also show a blue (B) contour away from cyclohexyl ring of the template molecule where low electron density is expected to increase the activity. The electronegative group SO$_2$ in **15** (IC$_{50}$ 200 nM) and **31** (IC$_{50}$ 260 nM) is oriented towards blue (B) contours; these molecules exhibit very low activity. The steric contours (Fig. 5) show a green (G) contour near cyclohexyl ring of the template molecule where bulky substituents are expected to increase the activity. The good inhibitory potency of **21** (IC$_{50}$ 4.1 nM), **22** (IC$_{50}$ 16 nM) and **23** (IC$_{50}$ 20 nM) are due to orientation of their cycloalkyl substituent towards sterically favoured green (G) contour. The steric contours also show a yellow (Y) contour near the ethylene linker of the template molecule. The molecule **13** (IC$_{50}$ 187 nM) exhibits low activity as the methyl group on the isooxazole ring is buried in the sterically unfavourable yellow contour. The 2-methoxy on the benzyl group of **10** (IC$_{50}$ 80 nM) is also oriented towards unfavourable yellow contour and exhibits low activity.

The CoMSIA results were obtained using the same structural alignment and same training and test set as defined in the CoMFA. The combination of steric, electrostatic and hydrophobic fields in CoMSIA gave the best results (Model 2), giving cross-validation correlation coefficient of 0.541, conventional correlation coefficient of 0.967 and predictive correlation coefficient of 0.59. The other combinations like (i) steric and electrostatic fields (Model 1) (ii) steric, electrostatic, hydrogen bond donor and hydrogen bond acceptor fields (Model 3), and (iii) all fields (Model 4) in CoMSIA also gave statistically significant models. The other combinations in CoMSIA gave statistically insignificant results (data not shown). The Model 1 shows negative predictive correlation coefficient, and hence is not used for further analysis. The Models 3 and 4 exhibit relatively lower cross-validated, conventional and predictive correlation coefficients compared to Model 2, the best amongst various fields combinations in CoMSIA. The Model 2 of CoMSIA was used for final analysis and predictions. The r^2 value of 0.983 during 100 runs of analysis [18,19] shows that the Model 2 is stable and statistically robust. The contributions of steric, electrostatic and hydrophobic fields are in ratio 2:4:4 (Table 2). Comparing this with the field contributions of CoMFA analysis, it is revealed that steric hydrophobic interactions could be an important factor for PDE IV inhibitory activity.

A comparison of the residuals of the models from CoMFA and CoMSIA is made to evaluate their predictive ability (Table 4). Molecule **6** shows high residual value and this may be due to the different orientation of the naphthalene ring in **6** with respect to the corresponding substituents in other test molecules. Considering the steric contours of CoMSIA (Model 2),

Table 2
Summary of CoMFA and CoMSIA statistics

Parameter	CoMFA	CoMSIA			
		SE Model 1	SHE Model 2	SEDA Model 3	SEHDA Model 4
r^2_{cv}	0.494	0.367	0.541	0.491	0.507
N	6	6	6	6	6
r^2	0.986	0.941	0.967	0.909	0.944
SEE	0.083	0.171	0.130	0.215	0.168
F-test value	253.04	56.06	101.9	34.9	59.49
Prob. of $r^2 = 0$	0.0	0.0	0.0	0.0	0.0
PRESS	0.587	1.40	0.554	0.681	0.77
r^2_{pred}	0.56	− 0.04	0.59	0.49	0.42
r^2_{bs}	0.992	0.970	0.983	0.955	0.977
SD	0.004	0.016	0.100	0.019	0.010
Contributions (%)					
Steric	0.601	0.325	0.192	0.262	0.169
Electrostatic	0.399	0.675	0.412	0.231	0.173
Hydrophobic			0.397		0.229
Donor				0.082	0.071
Acceptor				0.425	0.358

r^2_{cv} = cross-validated correlation coefficient; N = number of components; r^2 = conventional correlation coefficient; SEE = standard error of estimate; PRESS = predicted residual sum of squares of test set molecules, r^2_{pred} = predictive correlation coefficient, r^2_{bs} = correlation coefficient after 100 runs of bootstrapping analysis, SD = standard deviation from 100 bootstrapping runs, S = steric field, E = electrostatic field, H = hydrophobic field, D = hydrogen bond donor field, A = hydrogen bond acceptor field.
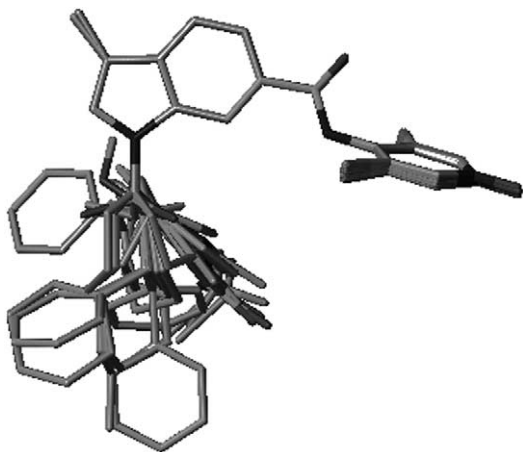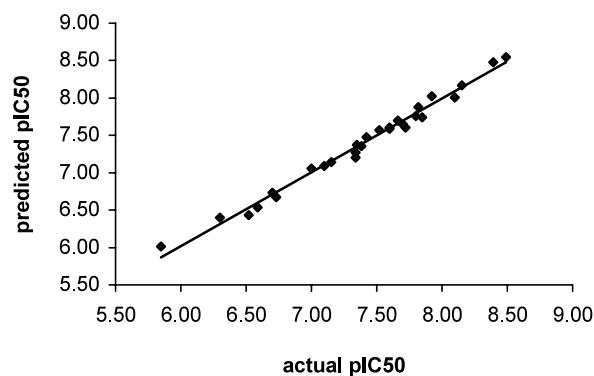

Fig. 1. Alignment of the training set molecules.

Fig. 2. Plot of predicted versus actual pIC50 values of training set molecules for CoMFA model.

green (G) contours indicate favourable regions while yellow (Y) contours indicate unfavourable regions for bulkier substituents. In the electrostatic contours, the introduction of electronegative substituents in red (R) regions may increase the affinity while in blue (B) regions decrease the affinity. In hydrophobic contours, magenta (M) regions favour hydrophobic groups while cyan (C) regions favour hydrophilic groups. The steric contours (Fig. 6a) produced by CoMFA and CoMSIA (Model 2) are similar. The electrostatic contours (Fig. 6a) produced by CoMFA and CoMSIA are quite different. The analysis of electrostatic CoMSIA contours shows presence of a red (R) contour near cyclohexyl ring of the template molecule and a blue (B) contour surrounding the red (R) contour. The
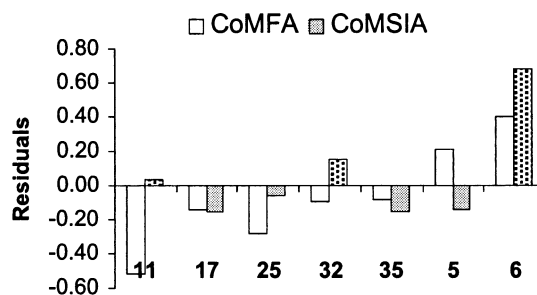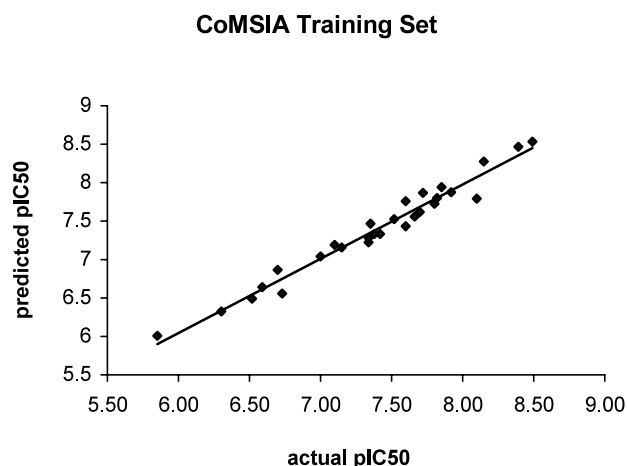

Fig. 3. Histogram of test set molecules.

CoMSIA Training Set

Fig. 4. Plot of predicted versus actual pIC50 values of training set molecules for CoMSIA model.

phenyl ring in the molecules **24** (IC$_{50}$ 8 nM) and **27** (IC$_{50}$ 7 nM) is oriented towards red (R) contour where electron density is favoured and hence they exhibit good activity. The electronegative oxygen in $-CO_2H$ of **34** (IC$_{50}$ 1400 nM) is oriented towards disfavouring blue (B) contour responsible for its low activity. The hydrophobic contours (Fig. 6b) show presence of two

small magenta (M) contours, one near the ethylene linker and the other away from the cyclohexyl ring of the template molecule, where the hydrophobic substituents may increase the activity. Two cyan (C) contours (Fig. 6b) are seen, one in the cyclohexyl ring of the template molecule and the other away from it, where the hydrophilic substituent may increase the activity.

The best CoMSIA model (Model 2) indicates that hydrogen bond donor and hydrogen bond acceptor fields do not improve the model. The CoMFA and CoMSIA models described are predictive enough to guide the design of new molecules.

3. Conclusions

The 3D-QSAR analyses, CoMFA and CoMSIA were used to build statistically significant models with good correlative and predictive power for PDE IV inhibitory activities of the indole derivatives. The initial geometry of the template molecule (**3**, the most active of the series) was obtained from the simulated annealing approach and was then used to derive remaining structures. The robustness of the derived models was verified by boot-strapping method. The combination of steric, electro-

Table 3
Actual, predicted inhibitory activities (pIC$_{50}$) and residuals of the training set molecules. (Model 2 was used for CoMSIA)

Molecule	Actual pIC$_{50}$	Predicted pIC$_{50}$		Residuals	
		CoMFA	CoMSIA	CoMFA	CoMSIA
1	7.82	7.88	7.80	−0.06	0.02
10	7.10	7.09	7.19	0.01	−0.09
12	7.92	8.02	7.88	−0.10	0.04
13	6.73	6.68	6.56	0.05	0.17
14	7.38	7.36	7.33	0.02	0.05
15	6.70	6.73	6.87	−0.03	−0.17
16	6.52	6.43	6.49	0.09	0.03
18	7.35	7.38	7.46	−0.03	−0.12
2	7.00	7.06	7.04	−0.06	−0.04
19	7.72	7.60	7.87	0.12	−0.15
20	7.52	7.57	7.52	−0.05	0.00
21	8.39	8.48	8.47	−0.09	−0.08
22	7.80	7.76	7.72	0.03	0.07
23	7.70	7.65	7.62	0.05	0.08
24	8.10	8.01	7.79	0.09	0.30
26	7.85	7.74	7.94	0.11	−0.09
27	8.15	8.16	8.27	−0.01	−0.12
28	7.34	7.27	7.23	0.07	0.11
29	7.66	7.67	7.56	−0.04	0.10
30	7.42	7.48	7.34	−0.06	0.08
31	6.59	6.54	6.64	0.05	−0.05
33	6.30	6.40	6.32	−0.10	−0.02
34	5.85	6.01	6.00	−0.16	−0.15
4	7.60	7.60	7.76	0.00	−0.16
7	7.15	7.14	7.16	0.01	0.00
8	7.60	7.59	7.43	0.01	0.17
9	7.34	7.21	7.29	0.13	0.05
3	8.49	8.54	8.53	−0.05	−0.04

Table 4
Actual, predicted inhibitory activities (pIC$_{50}$) and residuals of the test set molecules. (Model 2 was used for CoMSIA)

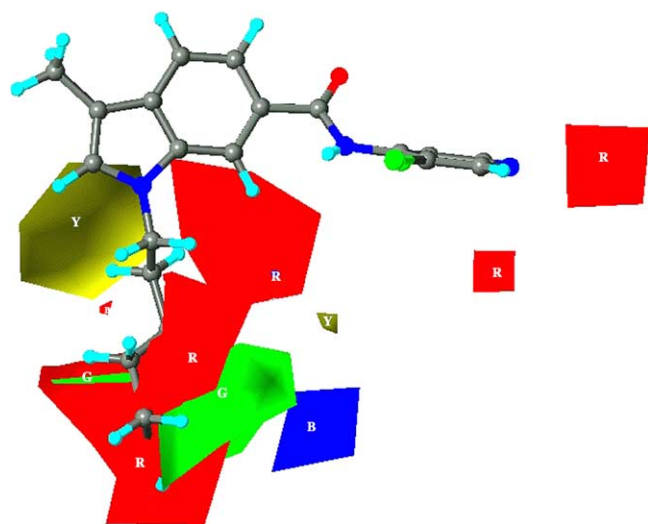| Molecule	Actual pIC$_{50}$	Predicted pIC$_{50}$		Residuals	
		CoMFA	CoMSIA	CoMFA	CoMSIA
11	7.22	7.74	7.19	−0.52	0.03
17	7.28	7.42	7.43	−0.14	−0.15
25	7.62	7.90	7.68	−0.28	−0.06
32	7.92	8.01	7.77	−0.09	0.15
35	7.10	7.18	7.25	−0.08	−0.15
5	7.74	7.53	7.88	0.21	−0.14
6	8.28	7.88	7.60	0.40	0.68

Fig. 5. The CoMFA steric and electrostatic contour maps. The most active molecule **3** is shown in the background. Red (R) colour is a negative charged region, blue (B) a positively charged region, green (G) a positive sterically active region, and yellow (G) a negatively sterically active region.

static and hydrophobic fields in CoMSIA gave the best results. Result of this study may provide an important basis for future drug design studies and synthesis of more potent PDE IV inhibitors against asthma.

4. Experimental

4.1. Dataset for analysis

Reported data on a series of indoles [10,11] were used (Table 1). The compounds were evaluated for PDE IV inhibition (IC50, nM) in macrophage homogenates via a two-step radio isotopic method [20]. Batches of PDE IV were obtained from guinea-pig macrophages [21]. The IC$_{50}$ values of 35 molecules were segregated into groups of 28 and 7 as training set and test set respectively such that the ratio of training set molecules to test set molecules would be in the approximate ratio 4:1. The training set of 28 molecules was represented by a combination of highly active (IC$_{50}$ 3–50 nM), moderately active (IC$_{50}$ 51–500 nM), and less active (IC$_{50}$ > 500 nM) molecules and test set of seven molecules was constituted by molecules having high and moderate activities.

The IC$_{50}$ values were converted into pIC$_{50}$ according to the formula,

$$pIC_{50} = -\log_{10} IC_{50}$$

4.2. Molecular modelling

The 3D-QSAR was performed using SYBYL 6.6 [22] installed on a Silicon Graphics Power ONYX *extreme* workstation. Since the crystal structure of PDE IV-inhibitor complex is not available, the least energy conformer was used as the bioactive conformation. The initial conformation of the most active analog **3** was obtained from simulated annealing as it enables the rapid identification of the global minimum energy conformer [23]. The system was subjected to simulated annealing by heating at 1000 K for 1 ps and then cooling at 200 K for 1 ps. The exponential annealing function was used and 10 such cycles were run. The least energy conformer obtained by this method was subjected to further minimization. The minimized conformer, thus obtained, was taken as the template and rest of the molecules were built from it. A constrained minimization followed by full minimization was carried out on these molecules in order to prevent the conformations moving to a false region. MMFF94 force field and partial atomic charges were used. Powell's conjugate gradient method was used for minimization. The gradient of 0.05 kcal mol^{-1} Å^{-1} was set as a convergence criterion.
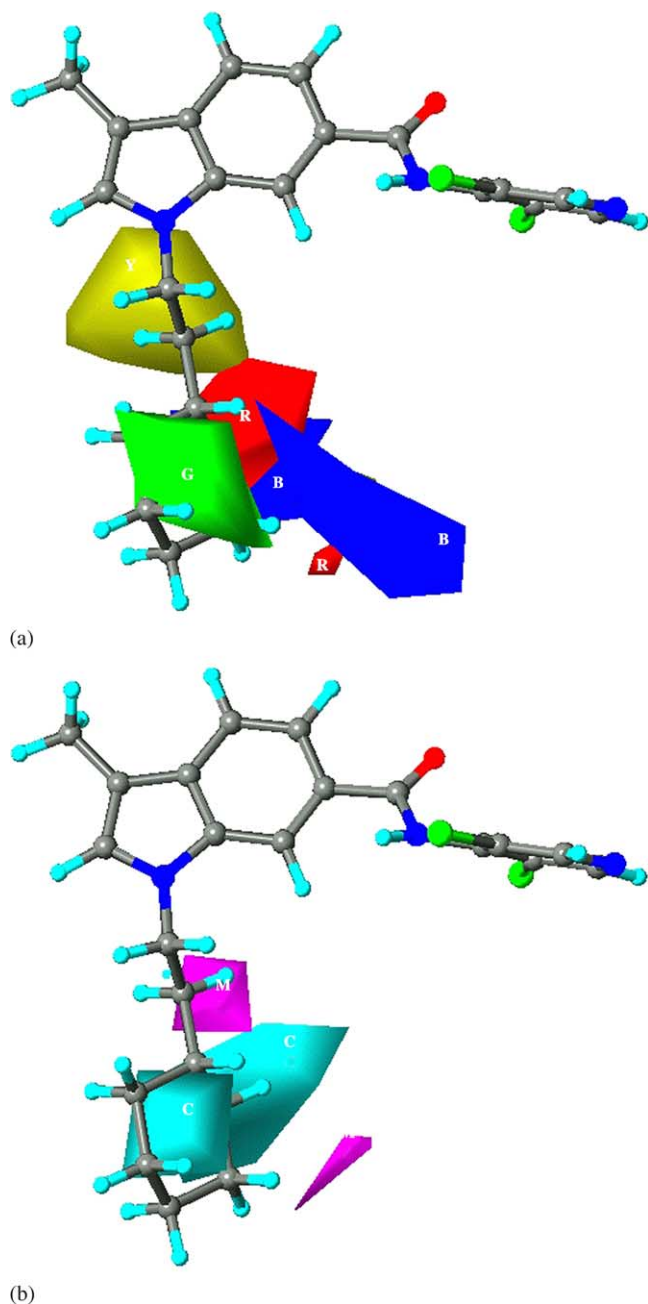
Fig. 6. The CoMSIA steric and electrostatic (a), and hydrophobic (b) contour maps. The most active molecule **3** is shown in the background. Red (R) colour represents the negative charge region, blue (B) is the positive charge region, green (G) is the more bulky region, yellow (Y) the less bulky region, magenta (M) the hydrophobic region and cyan (C) the hydrophilic region.

4.3. Alignment

The most crucial input for CoMFA is the alignment of the molecules. The template molecule **3** was taken and the rest of the molecules were aligned to it using the DATABASE ALIGNMENT method in the SYBYL. The molecules were aligned to the template molecule by using indole nucleus. The aligned molecules are shown in Fig. 1.

4.4. CoMFA interaction energy calculation

The steric and electrostatic CoMFA fields were calculated at each lattice intersection of a regularly spaced grid of 2.0 Å in all three dimensions within defined region. The van der Waals potential and coulombic term representing the steric and electrostatic fields respectively were calculated using standard Tripos force fields. A distance-dependent dielectric constant of 1.00 was used. An sp^3 carbon atom with +1.00 charge was used as a probe atom. The steric and electrostatic fields were truncated at +30.00 kcal mol^{-1}, and the electrostatic fields were ignored at the lattice points with maximal steric interactions.

4.5. CoMSIA interaction energy calculation

The steric, electrostatic, hydrophobic, hydrogen bond donor and hydrogen bond acceptor potential fields were calculated at each lattice intersection of a regularly spaced grid of 2.0 Å. A probe atom with radius 1.0 Å and +1.0 charge with hydrophobicity of +1.0 and hydrogen bond donor and hydrogen bond acceptor properties of +1.0 was used to calculate steric, electrostatic, hydrophobic, donor and acceptor fields. The contribution from these descriptors was truncated at 0.3 kcal mol^{-1}.

4.6. Partial least square (PLS) analysis

PLS method was used to linearly correlate the CoMFA fields to the inhibitory activity values. The cross-validation [24,25] analysis was performed using the leave one out (LOO) method in which one compound is removed from the dataset and its activity is predicted using the model derived from the rest of the dataset. The cross-validated r^2 that resulted in optimum number of components and lowest standard error of prediction were considered for further analysis. Equal weights were assigned to steric and electrostatic fields using COMFA_STD scaling option. To speed up the analysis and reduce noise, a minimum filter value σ of 2.00 kcal mol^{-1} was used. Final analysis was performed to calculate conventional r^2 using the optimum number of components. To further assess the robustness and statistical confidence of the derived models, bootstrapping analysis for 100 runs was performed. Bootstrapping involves the generation of many new data sets from original data set and is obtained by randomly choosing samples from the original data set. The statistical calculation is performed on each of these bootstrapping samplings. The difference between the parameters calculated from the original data set and the average of the parameters calculated from the many bootstrapping samplings is a measure of the bias of the original calculations. The entire cross-validated results were

analysed considering the fact that a value of r^2_{cv} above 0.3 indicates that probability of chance correlation is less than 5% [26].

4.7. Predictive correlation coefficient

The predictive ability of each 3D-QSAR model was determined from a set of seven compounds that were not included in the training set. These molecules were aligned, and their activities were predicted. The predictive correlation coefficient (r^2_{pred}), based on molecules of test set, is defined as,

$$r^2_{pred} = (SD - PRESS)/SD$$

where SD is the sum of the squared deviations between the biological activities of the test set and mean activities of the training set molecules and PRESS is the sum of squared deviation between predicted and actual activity values for every molecule in test set.

References

[1] M.J. Perry, G.A. Higgs, Curr. Opin. Chem. Biol. 2 (1998) 472–481.

[2] S.H. Soderling, J.A. Beavo, Curr. Opin. Cell. Biol. 12 (2000) 174–179.

[3] S. Domenico, Curr. Opin. Invest. Drugs 1 (2000) 204–213.

[4] M.A. Giembycz, Drugs 59 (2000) 193–212.

[5] V.D. Piaz, M.P. Giavannoni, Eur. J. Med. Chem. 35 (2000) 463–480.

[6] J.A. Beavo, M. Conti, R.J. Heaslip, Mol. Pharmacol. 46 (1994) 399–405.

[7] M. Marivet, J. Bourguignon, C. Lugnier, A. Mann, J. Stoclet, C. Wermuth, J. Med. Chem. 32 (1989) 1450–1457.

[8] M.J. Asthon, D.C. Cook, G. Fenton, J. Karlsson, M.N. Palfreyman, D. Raesburn, A.J. Ratcliffe, J.E. Souness, M.N. Thurairatnam, N. Vicker, J. Med. Chem. 37 (1994) 1696–1703.

[9] C. Burnouf, M. Pruniaux, Curr. Pharm. Des. 8 (2002) 1255–1296.

[10] C. Hulme, K. Moriarty, B. Miller, R. Mathew, M. Ramanjulu, P. Cox, J. Souness, K.M. Page, J. Uhl, J. Travis, F. Huang, R. Labaudiniere, S.W. Djuric, Bioorg. Med. Chem. Lett. 8 (1998) 1867–1872.

[11] C. Hulme, K. Moriarty, B. Miller, R. Mathew, M. Ramanjulu, P. Cox, J. Souness, K.M. Page, J. Uhl, J. Travis, F. Huang, R. Labaudiniere, S.W. Djuric, Bioorg. Med. Chem. Lett. 8 (1998) 3053–3058.

[12] R.H. Xu, A.M. Hassel, D. Vanderwaal, M. Lambert, W. Holmes, M. Luther, W. Rocque, M. Milburn, Y. Zhaso, H. Ke, R.T. Nolte, Science 288 (2000) 1822–1825.

[13] A.K. Chakraborti, B. Gopalakrishnan, M. Sobhia, A. Malde, Bioorg. Med. Chem. Lett. 13 (2003) 1403–1408.

[14] R.D. Cramer, III, D.E. Patterson, J.D. Bunce, J. Am. Chem. Soc. 110 (1988) 5959–5967.

[15] G.R. Desiraju, B. Gopalakrishnan, R.K. Jetti, A. Nagaraju, D. Raveendra, J.A. Sarma, M.E. Sobhia, R. Thilagavathi, J. Med. Chem. 45 (2002) 4847–4857.

[16] G.R. Desiraju, J.A. Sarma, D. Raveendra, B. Gopalakrishnan, R. Thilagavathi, M.E. Sobhia, H.S. Subramanya, J. Phys. Org. Chem. 14 (2001) 481–487.

[17] G. Klebe, U. Abraham, T. Mietzner, J. Med. Chem. 37 (1994) 4130–4146.

[18] R.D. Cramer, J.D. Bunce, D.E. Patterson, Quant. Struct.–Act. Relat. 7 (1988) 18–25.

[19] V.S. Murthi, V.M. Kulkarni, Bioorg. Med. Chem. 10 (2002) 2267–2282.

[20] W.J. Thompson, W. Teraski, P.M. Epstein, S.J. Strada, Adv. Cyclic Nucleotide Res. 10 (1979) 69–92.

[21] N.C. Turner, L.J. Wood, F.M. Burns, T. Gueremy, J. Souness, Br. J. Pharmacol. 108 (1993) 4876–4883.

[22] SYBYL 6.6 is available from Tripos Associates Inc., 1699 S Hanley Rd., St. Louis, MO 631444, USA.

[23] M.T. Barakat, P.M. Dean, J. Comput.-Aided. Mol. Des. 4 (1990) 295–316.

[24] T. Halgren, J. Am. Chem. Soc. 112 (1990) 4710–4723.

[25] B.L. Podlogar, D.M. Ferguson, Drug Des. Discov. 17 (2000) 4–12.

[26] M. Clark, R.D. Cramer, III, D.M. Jones, D.E. Patterson, P.E. Simeroth, Tetrahedron Comput. Methodol. 3 (1990) 47–59.